Identification and nanomechanical characterization of the fundamental single-strand protofilaments of amyloid α-synuclein fibrils

Francesco Simone Ruggeri[a,b,1], Fabrizio Benedetti[c], Tuomas P. J. Knowles[b,d], Hilal A. Lashuel[e], Sergey Sekatskii[a], and Giovanni Dietler[a,1]

[a]Laboratory of Physics of Living Matter, École Polytechnique Fédérale de Lausanne (EPFL), 1015 Lausanne, Switzerland; [b]Department of Chemistry, University of Cambridge, CB2 1EW Cambridge, United Kingdom; [c]Centre for Integrative Genomics, Faculty of Biology and Medicine, University of Lausanne, 1015 Lausanne, Switzerland; [d]Cavendish Laboratory, Department of Physics, University of Cambridge, CB3 0HE Cambridge, United Kingdom; and [e]Laboratory of Molecular and Chemical Biology of Neurodegeneration, Brain Mind Institute, Faculty of Life Sciences, École Polytechnique Fédérale de Lausanne (EPFL), 1015 Lausanne, Switzerland

Edited by Ehud Gazit, Tel Aviv University, Tel Aviv, Israel, and accepted by Editorial Board Member F. Ulrich Hartl May 23, 2018 (received for review December 6, 2017)

The formation and spreading of amyloid aggregates from the presynaptic protein α-synuclein in the brain play central roles in the pathogenesis of Parkinson's disease. Here, we use high-resolution atomic force microscopy to investigate the early oligomerization events of α-synuclein with single monomer angstrom resolution. We identify, visualize, and characterize directly the smallest elementary unit in the hierarchical assembly of amyloid fibrils, termed here single-strand protofilaments. We show that protofilaments form from the direct molecular assembly of unfolded monomeric α-synuclein polypeptide chains. To unravel protofilaments' internal structure and elastic properties, we manipulated nanomechanically these species by atomic force spectroscopy. The single-molecule scale identification and characterization of the fundamental unit of amyloid assemblies provide insights into early events underlying their formation and shed light on opportunities for therapeutic intervention at the early stages of aberrant protein self-assembly.

amyloid | protein aggregation | atomic force microscopy | early molecular assembly | force spectroscopy

The aggregation of α-synuclein into cross–β-sheet fibrillar structures plays a central role in the neuropathology of Parkinson's disease (PD) and other neurodegenerative diseases (Synucleinopathies) (1–6). Despite the widespread association of α-synuclein aggregation with the formation of Lewy bodies, the brain pathology that characterizes PD, the mechanistic roles of α-synuclein oligomerization and fibril formation in cell death and disease onset have remained challenging to identify (7). In particular, the nature of the specific state(s) of proteins that cause cytotoxicity is not well established. It is clear, however, that aggregated rather than monomeric forms of α-synuclein are primarily implicated in α-synuclein–mediated toxicity and pathology spreading in PD and related Synucleinopathies (3).

The kinetics of α-synuclein aggregation follows a nucleation-dependent process, where monomers initially aggregate into oligomeric species leading to the final formation of the amyloid fibrillar aggregates (8–10). The kinetics and rates of α-synuclein aggregation, as well as the morphologies of the different aggregates it populates on the pathway to amyloid formation, are strongly influenced by the experimental conditions used. In particular, incubation under shaking condition or in the presence of lipids is known to accelerate the fibril formation process (4, 11). Increasing evidence suggests that the prefibrillar aggregates, such as oligomers and protofibrils, or the process of fibrillization, rather than the final mature fibrillar products, are responsible for α-synuclein toxicity in vivo (12–14).

Although the ability to reproduce α-synuclein fibril formation in vitro has advanced our understanding of the molecular and structural determinants of α-synuclein aggregation and pathology onset, our understanding of early oligomerization events and the mode and strength of monomer interactions at different stages of the amyloid pathway remains very limited. For these reasons, the identification and characterization of aggregation intermediates on the pathway to α-synuclein amyloid formation is fundamental to understanding the mechanisms of amyloid formation, identification of the toxic species, and the development of novel diagnostic and therapeutic strategies for PD and related disorders.

Atomic force microscopy (AFM) and single-molecule force spectroscopy represent important research tools for achieving quantitative understanding of the mechanism of amyloid formation and characterization of different species on the amyloid pathway at the single-molecule scale (15–19). Several AFM studies suggested that many amyloidogenic proteins follow a hierarchical assembling model in which a certain number of elongated prefibrillar species with nanometer-size diameters and micrometer-scale lengths, termed protofilaments, intertwine or

Significance

Today, more than 40 million people worldwide are affected by neurodegenerative disorders. These diseases are associated at the molecular level with the aggregation of specific proteins into insoluble fibrils, termed amyloids. Increasing evidence suggests that the intermediate aggregates, rather than the final fibrillar products, are implicated in toxicity in vivo. However, the investigation of the conversion of proteins into amyloids represents a formidable experimental challenge because of their nanoscale and heterogeneous nature. Here, we report the identification of a mechanism of early assembly of monomeric proteins into elongated intermediates during amyloid formation. The biophysical characterization of novel intermediate molecular species is fundamental to unravel their mechanism of formation and gain insights into their potential toxicity and role in pathology.

Author contributions: F.S.R., T.P.J.K., H.A.L., S.S., and G.D. designed research; F.S.R. and F.B. performed research; F.S.R., F.B., and T.P.J.K. analyzed data; and F.S.R., F.B., T.P.J.K., H.A.L., S.S., and G.D. wrote the paper.

The authors declare no conflict of interest.

This article is a PNAS Direct Submission. E.G. is a guest editor invited by the Editorial Board.

[1]To whom correspondence may be addressed. Email: fsr26@cam.ac.uk or giovanni.dietler@epfl.ch.

This article contains supporting information online at www.pnas.org/lookup/suppl/doi:10.1073/pnas.1721220115/-/DCSupplemental.

Published online June 25, 2018.

laterally associate to form the final mature amyloid fibrillar structures with a typical diameter in the order of 6–13 nm; this was also the case with α-synuclein (5, 20–26). Previous studies sought to quantify the structural, nanomechanical properties and the interaction forces of the protofilaments within mature amyloid fibrils (15–17). These studies demonstrated how single aggregate imaging and manipulation methods enable studying the mechanics and structural dynamics of amyloid inner properties and formation. However, to date, it has not been possible to isolate and characterize the earliest elementary units in the assembly process formed from a single beta-sheet. This difficulty has originated in large part from their transient nature and their expected very small dimensions with a thickness corresponding to a single strand. Thus, our current knowledge of their structural properties is based primarily on investigating their structure and morphology when already present within mature fibrils.

Here, we use high-resolution AFM and force spectroscopy to revisit the pathway of α-synuclein fibril formation, with special emphasis on early molecular assembly events, to identify and characterize the elemental protofilament unit leading to the formation of mature fibrillar amyloids. We report the detection and characterization of the smallest elementary unit in the hierarchical assembly of amyloid fibrils of α-synuclein, which assembles directly from unfolded monomers termed here single-strand protofilaments. These protofilaments possess a subnanometer-scale cross-sectional diameter which is smaller than previously observed aggregated species of α-synuclein. Indeed, their subnanometer diameter is smaller than the typical dimensions of previously observed elongated nonmature aggregated species of α-synuclein [diameter of about 3–6 nm (5)], much smaller than the typical dimensions of mature amyloid fibrils (diameter of about 6–13 nm), and have a radius of gyration smaller than an individual monomer itself (~3 nm) (5, 24). The application of a scale reasoning demonstrates that the single-strand protofilament species are directly assembled from monomers of α-synuclein, and with a height corresponding to a single strand. Finally, we performed atomic force spectroscopy studies to characterize directly the inner mechanical, structural, and thermodynamical properties of single-strand protofilaments by means of statistical theory of biopolymers. We show that when subjected to mechanical dissection, the single-strand protofilaments unravel into components showing an average persistence length consistent with the elastic properties of a polymer chain composed of unstructured monomers of α-synuclein, as predicted by their cross-sectional dimensions.

Results and Discussion

Aggregation of α-Synuclein Proceeds Through Formation of Protofilament Aggregates. To unravel the process of α-synuclein fibrillization at the single-molecule scale, we exploited AFM high-resolution 3D morphology imaging with the deposition of the negatively charged α-synuclein protein on both an atomically flat negative mica and on a positively functionalized mica substrate (mica-APTES) (Fig. 1 and *SI Appendix*, Fig. S1) (27). We incubated freshly filtered (100 kDa) α-synuclein monomeric solution in vitro under shaking conditions at 37 °C for 10 d. We collected an aliquot of the solution at 0, 1, and 10 d, and then we deposited an aliquot of each sample on the substrate to acquire morphology maps of the sample by AFM. The sample was monitored in parallel

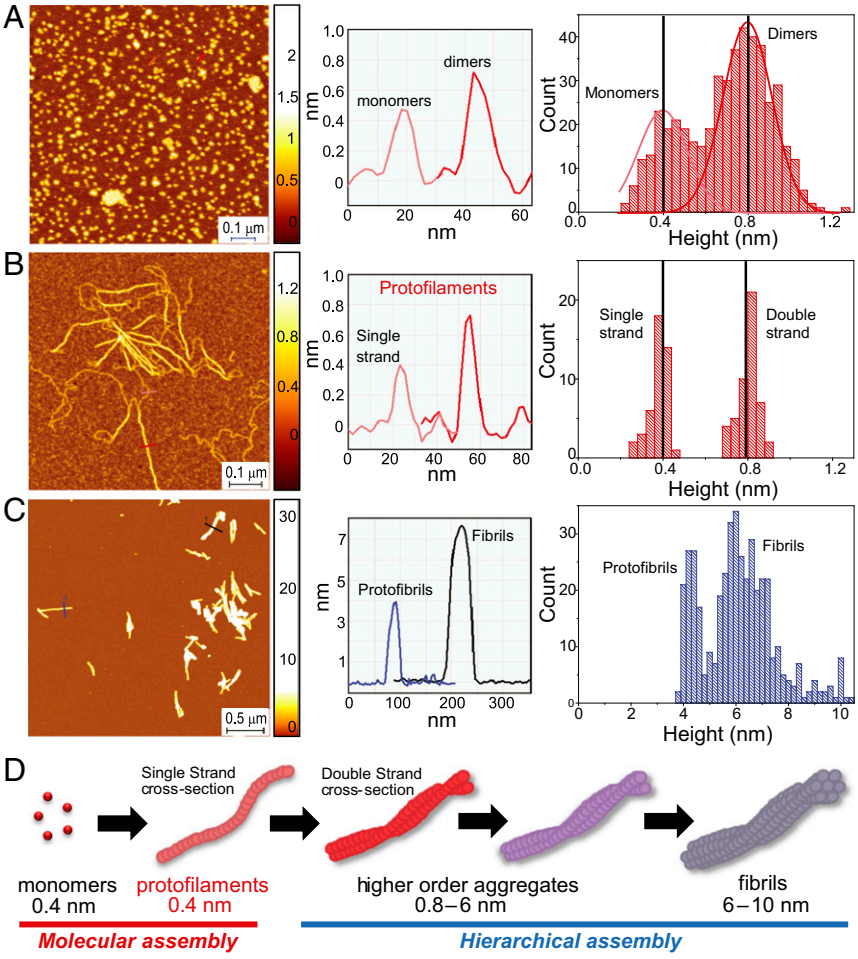

Fig. 1. α-Synuclein fibrillization under shaking conditions. (*A*–*C*) Aggregation time course monitored by high-resolution AFM imaging, detail of the cross-sectional height of a species and single-molecule statistical analysis, with histogram distributions of the cross-sectional height of the species observed at (*A*) 0, (*B*) 1, and (*C*) 10 d (Z scales are in nanometers). (*D*) Model of α-synuclein fibril formation showing the (*i*) initial molecular assembly leading to the formation of the newly identified single-strand protofilaments (in light red) and (*ii*) subsequent hierarchical assembly leading to the formation of mature amyloid fibrils. At the bottom, the typical AFM height of each species is indicated.

by circular dichroism and thioflavin T to independently confirm the state of aggregation in bulk, as we previously reported (27, 28).

Before incubation and immediately after the dissolution of α-synuclein in buffer, only monomers and early oligomers were present on the surface and no fibrillar species were visible (Fig. 1*A* and *SI Appendix*, Fig. S2) (27, 28). A single-molecule statistical analysis revealed that the smallest oligomeric population had a cross-sectional height of 0.3–0.4 nm (Fig. 1*A*). The height of this first population corresponded to the height on a surface of a monomeric polypeptide chain, as previously measured for an unfolded or partially folded protein by scanning probe microscopy (27, 29, 30). Thus, the first oligomeric population corresponded to monomeric α-synuclein (*SI Appendix*). In the histogram distribution of height of the early oligomeric populations, we also observed another population with double the cross-sectional height of the monomeric species, which we associated to dimeric species. After 24 h of incubation, we could observe the formation of elongated protofilaments species having subnanometer-scale diameter and micrometer-scale length (Fig. 1*B*). We observed two polymorphs of the protofilament species. The first species had a cross-sectional height of 0.3–0.4 nm, corresponding to the height of monomeric α-synuclein. The second species had a cross-sectional height of 0.7–0.9 nm, which corresponded to the cross-sectional height of dimers (Fig. 1 *A* and *B*). Remarkably, we reported the observation of subnanometer fibril-like aggregates of α-synuclein. We termed their elemental unit, possessing the smallest cross-sectional diameter of a single monomer (0.3–0.4 nm), as single-strand cross-section protofilaments or more easily single-strand protofilaments (Fig. 1*B*). Considering that the second polymorphic population had double the height of single-strand protofilaments, we termed them double-strand cross-section protofilaments. Finally, after 10 d of incubation, we observed the formation of higher order aggregates and mature amyloid fibrils of α-synuclein with height ranging between 4–6 and 6–9 nm, respectively (Fig. 1*C*). This observation suggested that the protofilaments species were on-pathway of the formation of mature fibrils [i.e., height by AFM of 6–9 nm (24)]. As depicted in Fig. 1*D*, our results suggested that the early aggregation of α-synuclein proceeded through the molecular assembly of monomers into the single-strand protofilaments, which then interact and assemble hierarchically to form higher order aggregates leading to the formation of mature amyloid fibrils.

Under shaking conditions, α-synuclein fibrillization occurred within 10 d, whereas several months of incubation are required to achieve complete fibrillation of α-synuclein under quiescent conditions (4, 27, 28). To investigate the process of protofilament formation with higher time resolution, we studied the aggregation of α-synuclein under quiescent conditions at 37 °C, over a long period of 181 d (Fig. 2). To avoid any bias for aggregation in our experimental setup, at each time point, we deposited an aliquot, of α-synuclein solution aggregated in vitro, on two substrates with the opposite state of charge: negative bare mica and positive mica-APTES (*SI Appendix*, Fig. S3). Analysis of the freshly prepared α-synuclein samples showed that they contain predominantly monomeric protein, and some oligomeric species were also observed (Fig. 2*A*). In static conditions, protofilament species were first observed after 2 months (Fig. 2*B*, 60 d) of incubation in vitro. Then, they elongated and increased in number and length after 6 months of incubation (Fig. 2*C*, 181 d). The kinetics of aggregation was confirmed independently on bare mica and functionalized mica-APTES substrates (Fig. 2*C* and *SI Appendix*, Fig. S3). Furthermore, we independently detected the protofilaments, after 180 d of incubation, by transmission electron microscopy (TEM) (Fig. 2*D*). AFM high-resolution imaging enabled observing that the double-strand protofilaments formed from the association of individual single-strand protofilaments (Fig. 2*E*). Similarly to shaking conditions, a statistical characterization of the cross-sectional dimensions of individual protofilament species showed that they could be separated in two main families according to their AFM

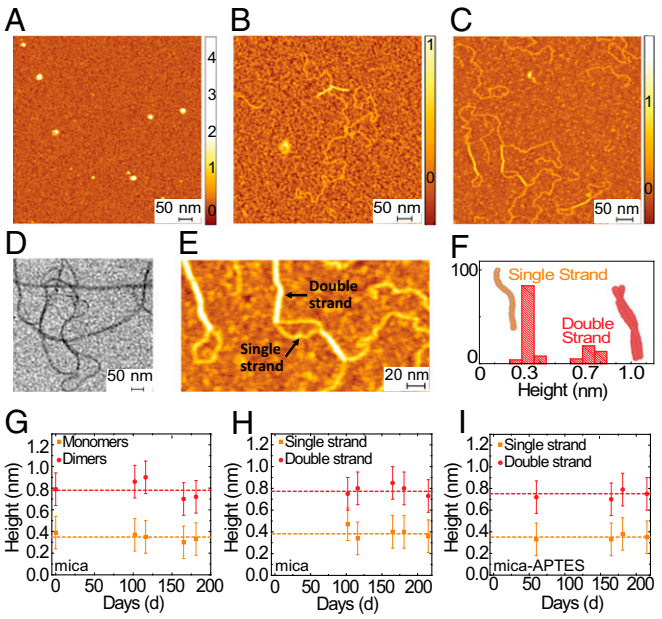

Fig. 2. Slow aggregation in quiescent conditions of monomeric α-synuclein into protofilament species. AFM image of (*A*) monomers and oligomers covering the surface at 0 d, (*B*) protofilaments after 60 d and (*C*–*E*) after 181 d as observed by (*C*) AFM and (*D*) TEM. (*E*) Detail of intertwining protofilaments. (*F*) Single-molecule statistical analysis and histograms of the cross-sectional height of protofilaments after 181 d. Comparison of the cross-sectional height of (*G*) the smallest oligomeric populations, corresponding to monomers and dimers, with the cross-sectional height of protofilaments on (*H*) bare mica and (*I*) mica-APTES as a function of the incubation time in vitro. (Z scales are in nanometers; error bar is 1 SD.)

height. The first family was corresponding with the single-strand protofilaments, with an average height of 0.3–0.4 nm, and the second family was corresponding with the double-strand protofilaments, which had an average height of 0.7–0.8 nm (Fig. 2*F*). The slow speed of aggregation in static conditions enabled monitoring, over a long period of time, the relationship between the height of monomers and dimers with the height of single- and double-strand protofilaments (Fig. 2 *G*–*I*). Independently from the incubation time, similarly as observed at time 0 d, the smallest oligomeric population possessed a cross-sectional height of ∼0.3–0.4 nm, while the second smallest dimeric population had a cross-sectional height of ∼0.6–0.9 nm (Fig. 2*G*). Correspondingly, within the time period investigated here, the two protofilament families showed identical cross-sectional height, of ∼0.4 nm and 0.8 nm, respectively. To rule out any possible effect of the surface of deposition on the morphological properties of the protofilaments, we deposited the sample solution on the two substrates with the opposite state of charge, negative mica (Fig. 2*H*) and positive mica-APTES (Fig. 2*I*). The protofilaments showed identical properties on mica and mica-APTES (*SI Appendix*, Fig. S3). Thus, the surface of deposition did not affect the structural properties of the protofilaments.

The AFM imaging combined with a single-molecule statistical analysis of the average heights of oligomeric and protofilaments species at different time points (Fig. 2 *G*–*I*) demonstrate that a single-strand protofilament possesses the same cross-sectional height of a monomer (orange dashed line), whereas a double-strand protofilament, formed from two single strands interacting, has the same cross-sectional height of the dimeric population (red dashed line).

Single-Strand Protofilaments Are Assembled Monomeric Chains. In both quiescent and shaking incubation conditions, the height of single-strand protofilaments corresponded to the height of a

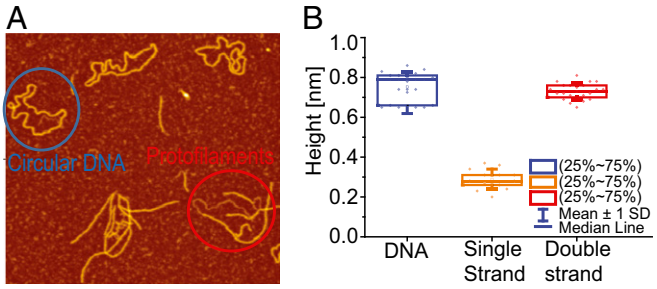

Fig. 3. Calibration of single-strand protofilament height relative to circular double-strand DNA. (*A*) AFM image of protofilaments and circular DNA (Z scale is in nanometers). (*B*) Scatter plot and comparison of the height of circular DNA and protofilaments.

single polypeptide chain. We measured an average height of 0.3–0.4 nm for both monomers and single-strand protofilaments (Figs. 1 and 2 and *SI Appendix*, Fig. S2). The measurement of height by AFM, in air for a relaxed object on a surface smaller than a couple of nanometers in height, could be affected by underestimation (*SI Appendix*) (31, 32). Thus, we deposited our protofilament aggregates together with circular DNA, which was used as an internal ruler for the measurement of the protofilament's real height (Fig. 3*A*). Indeed, DNA structure has been extensively studied and it is universally accepted as a flexible double helix with a ∼2-nm diameter. AFM measurements of DNA, in the same scanning conditions as for the protofilament imaging, showed a measured height of ∼0.8–1 nm (Fig. 3*B*), consistent with previous reports (32, 33). Single-strand structures possessed almost one half of the measured height of DNA molecules, whereas double-strand protofilaments had nearly the same height as DNA (Fig. 3*B*). Supposing that DNA and the aggregates have a similar geometrical cross-section shape, we could conclude that the real diameter of single-strand protofilaments was of ∼0.6–1 nm. The height of single-strand protofilaments was much smaller than the radius of gyration of a single monomer in globular conformation (2–3 nm) and of the order of the experimentally measured height of a single polypeptide chain (30). In addition, the protofilament species had a much smaller dimension of any previously observed aggregated species of α-synuclein. In fact, their subnanometer diameter is smaller than the typical dimensions of previously observed elongated nonmature (4–6 nm height) and mature (6–10 nm) amyloid aggregated species of α-synuclein (Fig. 1*D*) (5, 24). Hence, the subnanometer cross-sectional height of single-strand protofilaments excluded the possibility that more than one monomer was present within their cross-section. Besides, the protofilament's length, in the order of hundreds of nanometers, well exceeds the one of a fully extended monomeric chain of α-synuclein (∼50 nm, 0.35 nm for amino acid). Thus, we concluded that the protofilaments consisted of assembled polypeptide chains of monomers of α-synuclein in series.

Nanomechanical Manipulation of Protofilaments by Atomic Force Spectroscopy. The small cross-sectional diameter of protofilament species (<1 nm) did not permit the use of the well-established single-molecule methods, such as AFM-based nanoindentation and infrared nanospectroscopy, to probe their biophysical properties at the single-molecule scale (34, 35). For this reason, we pursued a nanomechanical manipulation of the protofilaments by means of atomic force spectroscopy (Fig. 4). The tip of our AFM cantilever was approached against the substrate, where protein aggregates were deposited. Then, it was retracted and force extension curves were recorded. The investigation of the spectroscopic force response for oligomeric and protofilament species showed a remarkable difference (*SI Appendix*, Fig. S4). At time 0 d, in the force spectra, there was no presence of any complex or repeatable force response. Conversely, after 181 d of incubation, highly reproducible multiple force plateaus (Fig. 4 and *SI Appendix*) forming a staircase-like picture were observed in the force–distance curves. These constant force-pulling events had a much longer length (up to 400 nm) than a fully extended α-synuclein monomeric polypeptide chain (∼50 nm). Therefore, the force plateaus were due to the presence of the two types of protofilaments on our surface, and as in previous studies, we associated the constant force-pulling events to the detaching of the protofilaments from the surface (15, 16). We present in Fig. 4*A* a model of the simplest possible detachment event from the surface (15–17). Initially, the AFM tip was approached on the substrate and it was capable of breaking a protofilament (Fig. 4 *A*, *1*). Indeed, as already measured and clearly demonstrated in the case of mature amyloid structures, which are notably stiffer than monomeric structures, ∼500 pN were already sufficient to break by indentation the aggregate (36). Then, the tip was moved far from the surface, and we started pulling the protofilament and detaching it from the substrate (Fig. 4 *A*, *2*) until the nanomechanical contact is lost (Fig. 4 *A*, *3*). In addition to the detachment of a single protofilament, several mechanical responses were measured during the process of protofilaments pulling from the surface (*SI Appendix*, Figs. S4 and S5). We focused our attention on the force plateaus (Fig. 4 *B*–*D*), which constituted the majority of the events (89%) compared with the nonspecific effects (11%). More specifically, we characterized the force plateau's length and height distribution. We performed a statistical analysis of the plateaus' lengths to prove that force plateaus were shorter than the actual protofilament's length (*SI Appendix*, Fig. S6). The force plateaus possessed an average length of ∼70 nm (Fig. 4*E*), whereas the protofilaments had a length with an average value of ∼170 nm (Fig. 4*F*). Then, to quantify the process of protofilaments' detachment from the surface and to obtain an experimental estimation of the forces involved, we measured the height of the observed plateau force steps. We measured the force

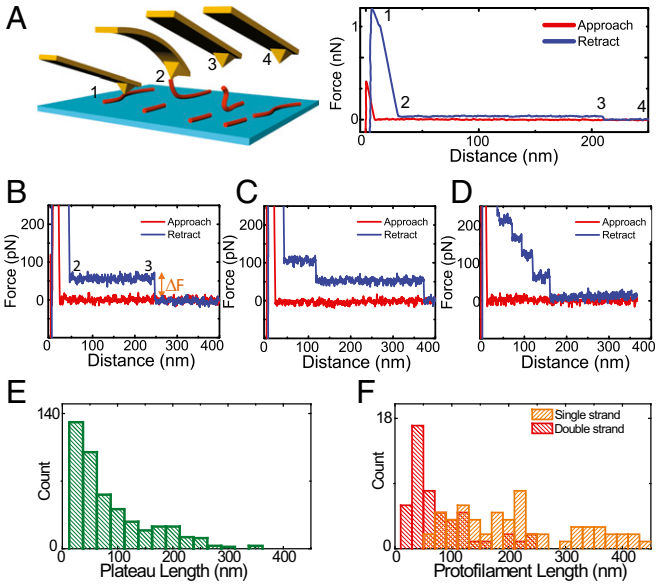

Fig. 4. Force responses of manipulated α-synuclein protofilaments. (*A*) Model of single protofilament's pulling and relative force–distance curve. (*1*) AFM tip is strongly pressed against a protofilament. (*2*) The strong pressure causes polymer breaking and a constant force plateau due to its unzipping from the surface. (*3*) Tip–filament contact is lost during the pulling. (*4*) Tip return to the initial position. (*B*) Single force plateau due to the pulling of one protofilament. (*C*) Double plateau due to the pulling of two protofilaments. (*D*) Pulling of four protofilaments. (*E*) Distribution of the lengths of constant force pulling events (plateaus). (*F*) Distribution of the lengths of protofilaments.

difference ΔF between the average height of a plateau and the baseline in the force curve (Fig. 4*B*). A distribution plot of this quantity showed a multimodal distribution with four peaks and some more rare higher force events, which we considered generically as the fifth peak (*SI Appendix*, Fig. S7*A*). The force peaks appeared at integer multiples of a single detachment event value of ∼50 pN (*SI Appendix*, Fig. S7*B*). We could extract an average quantized value of detachment force from the substrate of 57 ± 7.5 pN (*SI Appendix*, Fig. S7 *C* and *D*). Since single-strand protofilaments were longer and more abundant than double-strand ones (Fig. 4*F*), the pulling or unzipping of double-strand protofilaments could bring only a negligible broadening of the force distribution peaks and could be neglected (*SI Appendix*).

The quantized values of force plateaus obeyed a linear law, demonstrating that multiple plateaus were linked to the multiple detachments of several protofilaments from the surface. A Monte Carlo simulation of the process, modeling the breaking of n parallel bonds from the surface, explained to good approximation the essential features of this quantization and reproduced the measured experimental values, thus confirming that the presence of n plateaus was due to the nanomechanical detachment from the surface of n protofilaments in parallel (*SI Appendix*, Fig. S7 *C* and *D*).

Single-Strand Protofilaments Have Disordered Structural Organization. Remarkably, we observed two classes of force plateaus. The first class were flat constant force curves, while the second class were constant force plateaus with stretching events, which were observed inside or at the border of a plateau (*SI Appendix*, Fig. 6 *A–C*). Thus, after the characterization of the detachment process of the plateaus, we focused our attention on the plateaus presenting stretching events.

The quantization of the force plateaus (*SI Appendix*, Fig. S7) enabled us to exclude any internal unzipping of the protofilaments; thus, we concluded that during the pulling the protofilament species were simply manipulated and detached from the surface. This observation was in agreement with the above demonstrated conclusion (Figs. 1–3) that single-strand protofilaments have cross-sectional dimensions just of the order of the carbon–nitrogen backbone of a single α-synuclein monomer. The typical value of the length of the stretching events was of 15 ± 10 nm; the stretching events were in all cases <40 nm (n = 35) and smaller than the maximal extension of a single polypeptide chain of α-synuclein (∼50 nm; 0.35 nm for the amino acid). Thus, we could associate the stretching events to the elastic deformation of the carbon–nitrogen backbone of a single monomeric-like chain inside a protofilament (Fig. 5*D*). We investigated the nature of the stretching events by means of the statistical theory of biopolymers to retrieve the internal mechanical properties of the monomers within the aggregates (37). By fitting the stretching events with a worm-like chain model (WLC; see *SI Appendix*, Eq. **S2**), we could determine an internal average persistence length A of the single-strand protofilaments of A = 0.29 ± 0.16 nm (n = 35). This value was fully consistent with the persistence length of an unfolded protein (38). It was also already measured by AFM force spectroscopy that, upon similar stretching by AFM, mature amyloid fibrils formed by the glucagon peptide have an average internal persistence length of 0.70 ± 0.15 nm (17). Remarkably, the internal persistence length measured for mature fibrils was more than twice as big as in the case of the single-strand protofilaments.

Furthermore, we exploited the force curves in Fig. 5 *A–C* to measure the thermodynamic free energy change upon stretching of an α-synuclein monomer within the single-strand protofilaments. First, we measured the irreversible work (W) needed to stretch and deform the polypeptide chain. The integration of the area below the stretching events enabled us to measure an average value of W = 350 ± 100 kJ/mol. Then, we calculated the entropic term of the free energy necessary to separate the ends

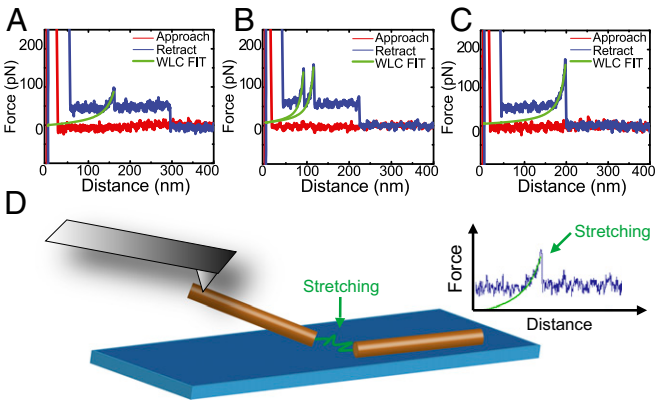

Fig. 5. Characterization internal nanomechanical properties of protofilaments through stretching. (*A*) Constant force plateau with a stretching event inside, (*B*) constant force plateau with two stretching events inside, and (*C*) force plateau preceded by a stretching event, fitted by the WLC model. (*D*) Schematic representation of protofilament internal stretching.

of the flexible chain by a distance z, as previously reported in the literature (37, 39). We obtained an average value of F_E = 40 ± 20 kJ/mol. We considered the irreversible work W done on the system the upper limit of the free energy change of protofilaments upon stretching, while we considered the entropic part of the free energy F_E the minimal free energy change upon the extension of the monomeric chain. Thus, when submitted to irreversible stretching, we could estimate that the free-energy change of a single-strand protofilament ranges between approximately $F \sim$ 40 and 350 kJ/mol. As expected, the irreversible work done to stretch a monomer is higher than its change of entropic free-energy F_E upon extension. Since the extended conformation of the polypeptide chain of a monomer does not allow stable hydrogen bonding, the irreversible work done to extend the chain can be likely related to the breaking of intramolecular hydrogen bonds (30, 40–42). We estimate that the energy to extend the monomeric chain to break a single hydrogen bond is given by $E_H = F/n$, where F is the free energy and n the number of intramolecular hydrogen bonds. For simplicity, we consider the presence of 1 hydrogen bond for each amino acid (41, 43). For a total free energy of 350 kJ/mol and a stretching length of 15 nm, we obtained an average estimated value of the free energy to break a hydrogen bond of E_H = 8 ± 2 kJ/mol. This value is in excellent agreement with the reported value in the literature of the free energy necessary to break hydrogen bonding in a monomeric protein (44–47). Furthermore, the measured strength of hydrogen bonding in a monomer within the protofilament is remarkably smaller than the energy of an intermolecular hydrogen bond in amyloid fibrils (∼15–30 kJ/mol) (48–51).

In conclusion, the single-strand protofilament aggregates do not possess the typical mechanical and thermodynamic properties of mature amyloid fibrils and possess a less-rigid structure arising by the early molecular assembly of unfolded monomers.

Conclusions

In this study, we demonstrate that the early aggregation of α-synuclein first proceeds through the assembly of monomers into elongated chain-like aggregates with a cross-section of a single strand. These aggregated species are composed of a single chain of monomeric α-synuclein in series (single strand) and possess subnanometer diameter and up to micrometer scale length. Our results demonstrate that these intermediate species are the smallest observable elementary unit in the hierarchical assembly of amyloid fibrils. It is widely accepted that the intermediate products of the aggregation rather than the final mature fibrillar products could be

responsible for α-synuclein toxicity in vivo (8). "Oligomers" is a generic term to indicate a heterogeneous ensemble of amyloid intermediates, which are normally depicted as spheroidal or toroidal objects. Several reports in the literature indicate that size, shape, and structure of these species are strictly related to their toxicity (6, 52, 53). The understanding of the early molecular assembly of α-synuclein and the identification and characterization of a new elongated oligomeric intermediate is of fundamental importance, since its different biophysical properties could be related to different mechanisms of amyloid toxicity in vivo and could offer new opportunities for developing new therapeutic strategies targeting the early stages of the assembly process.

We describe an experimental approach that would enable investigating and comparing the interaction forces of amyloid aggregates on different surfaces, such as hydrophobic ones. Unraveling these forces is central to understanding the mechanism of amyloid fibril formation and its role in the pathogenesis of PD and Synucleinopathies. Finally, the values obtained for the molecular interaction forces within and between the protofilaments shed light on the thermodynamics of the early hierarchical amyloid assembling process, and could furthermore provide cues to unraveling the fibrillation process at surfaces, such as cell membranes.

Materials and Methods

Detailed information on the experimental methods can be found in the *SI Appendix*. α-Synuclein was produced in *Escherichia coli* and then purified by previously accepted protocols (54). AFM images and force spectroscopy curves were realized using a Nanoscope IIIa (Bruker Corp.) and NX10 (Park Systems). TEM imaging was performed on a Tecnai Spirit BioTWIN electron microscope.

ACKNOWLEDGMENTS. This work was supported by the Darwin College; the Swiss National Foundation for Science Grants 152958, P300P2_171219, and 200021_162767; and the European Research Council under the European Union's Seventh Framework Programme (FP7/2007-2013) through the ERC grant PhysProt (Agreement 337969).

1. Goedert M (1997) Familial Parkinson's disease. The awakening of alpha-synuclein. *Nature* 388:232–233.
2. Conway KA, Harper JD, Lansbury PT (1998) Accelerated in vitro fibril formation by a mutant alpha-synuclein linked to early-onset Parkinson disease. *Nat Med* 4: 1318–1320.
3. Uversky V, Eliezer D (2009) Biophysics of Parkinsons disease: Structure and aggregation of-synuclein. *Curr Protein Pept Sci* 10:483–499.
4. Giehm L, Lorenzen N, Otzen DE (2011) Assays for α-synuclein aggregation. *Methods* 53:295–305.
5. Khurana R, et al. (2003) A general model for amyloid fibril assembly based on morphological studies using atomic force microscopy. *Biophys J* 85:1135–1144.
6. Lashuel HA, Lansbury PT, Jr (2006) Are amyloid diseases caused by protein aggregates that mimic bacterial pore-forming toxins? *Q Rev Biophys* 39:167–201.
7. Lansbury PT, Lashuel HA (2006) A century-old debate on protein aggregation and neurodegeneration enters the clinic. *Nature* 443:774–779.
8. Knowles TPJ, Vendruscolo M, Dobson CM (2014) The amyloid state and its association with protein misfolding diseases. *Nat Rev Mol Cell Biol* 15:384–396.
9. Tuttle MD, et al. (2016) Solid-state NMR structure of a pathogenic fibril of full-length human α-synuclein. *Nat Struct Mol Biol* 23:409–415.
10. Bloch DN, Miller Y (2017) Study of molecular mechanisms of α-synuclein assembly: Insight into a cross-β structure in the N-termini of new α-synuclein fibrils. *ACS Omega* 2:3363–3370.
11. Flagmeier P, et al. (2016) Mutations associated with familial Parkinson's disease alter the initiation and amplification steps of α-synuclein aggregation. *Proc Natl Acad Sci USA* 113:10328–10333.
12. Lashuel HA, Overk CR, Oueslati A, Masliah E (2013) The many faces of α-synuclein: From structure and toxicity to therapeutic target. *Nat Rev Neurosci* 14:38–48.
13. Hong DP, Han S, Fink AL, Uversky VN (2011) Characterization of the non-fibrillar α-synuclein oligomers. *Protein Pept Lett* 18:230–240.
14. Mahul-Mellier AL, et al. (2015) Fibril growth and seeding capacity play key roles in α-synuclein-mediated apoptotic cell death. *Cell Death Differ* 22:2107–2122.
15. Kellermayer MS, et al. (2005) Reversible mechanical unzipping of amyloid beta-fibrils. *J Biol Chem* 280:8464–8470.
16. Karsai A, et al. (2006) Mechanical manipulation of Alzheimer's amyloid beta1-42 fibrils. *J Struct Biol* 155:316–326.
17. Dong M, et al. (2008) AFM-based force spectroscopy measurements of mature amyloid fibrils of the peptide glucagon. *Nanotechnology* 19:384013.
18. Kienle S, et al. (2014) Effect of molecular architecture on single polymer adhesion. *Langmuir* 30:4351–4357.
19. Krysiak S, Liese S, Netz RR, Hugel T (2014) Peptide desorption kinetics from single molecule force spectroscopy studies. *J Am Chem Soc* 136:688–697.
20. Adamcik J, et al. (2010) Understanding amyloid aggregation by statistical analysis of atomic force microscopy images. *Nat Nanotechnol* 5:423–428.
21. Kad NM, et al. (2003) Hierarchical assembly of β2-microglobulin amyloid in vitro revealed by atomic force microscopy. *J Mol Biol* 330:785–797.
22. Sunde M, et al. (1997) Common core structure of amyloid fibrils by synchrotron X-ray diffraction. *J Mol Biol* 273:729–739.
23. Fändrich M, Meinhardt J, Grigorieff N (2009) Structural polymorphism of Alzheimer Abeta and other amyloid fibrils. *Prion* 3:89–93.
24. Sweers KK, Segers-Nolten IM, Bennink ML, Subramaniam V (2012) Structural model for α-synuclein fibrils derived from high resolution imaging and nanomechanical studies using atomic force microscopy. *Soft Matter* 8:7215.
25. Bauer HH, et al. (1995) Architecture and polymorphism of fibrillar supramolecular assemblies produced by in vitro aggregation of human calcitonin. *J Struct Biol* 115: 1–15.
26. Kamgar-Parsi K, Hong L, Naito A, Brooks CL, 3rd, Ramamoorthy A (2017) Growth-incompetent monomers of human calcitonin lead to a noncanonical direct relationship between peptide concentration and aggregation lag time. *J Biol Chem* 292:14963–14976.
27. Khalaf O, et al. (2014) The H50Q mutation enhances α-synuclein aggregation, secretion, and toxicity. *J Biol Chem* 289:21856–21876.
28. Ruggeri FS, et al. (2015) Influence of the β-sheet content on the mechanical properties of aggregates during amyloid fibrillization. *Angew Chem Int Ed Engl* 54:2462–2466.
29. Deng Z, et al. (2012) A close look at proteins: Submolecular resolution of two- and three-dimensionally folded cytochrome c at surfaces. *Nano Lett* 12:2452–2458.
30. Dedmon MM, Lindorff-Larsen K, Christodoulou J, Vendruscolo M, Dobson CM (2005) Mapping long-range interactions in α-synuclein using spin-label NMR and ensemble molecular dynamics simulations. *J Am Chem Soc* 127:476–477.
31. Garcia R, Perez R (2002) Dynamic atomic force microscopy methods. *Surf Sci Rep* 47: 197–301.
32. Cerreta A, et al. (2012) FM-AFM constant height imaging and force curves: High resolution study of DNA-tip interactions. *J Mol Recognit* 25:486–493.
33. Watson JD, Crick FHC (1953) Molecular structure of nucleic acids; a structure for deoxyribose nucleic acid. *Nature* 171:737–738.
34. Ruggeri FS, et al. (2016) Nanoscale studies link amyloid maturity with polyglutamine diseases onset. *Sci Rep* 6:31155.
35. Ruggeri FS, et al. (2015) Infrared nanospectroscopy characterization of oligomeric and fibrillar aggregates during amyloid formation. *Nat Commun* 6:7831.
36. Smith JF, Knowles TP, Dobson CM, Macphee CE, Welland ME (2006) Characterization of the nanoscale properties of individual amyloid fibrils. *Proc Natl Acad Sci USA* 103: 15806–15811.
37. Bustamante C, Smith SB, Liphardt J, Smith D (2000) Single-molecule studies of DNA mechanics. *Curr Opin Struct Biol* 10:279–285.
38. Rief M, Gautel M, Oesterhelt F, Fernandez JM, Gaub HE (1997) Reversible unfolding of individual titin immunoglobulin domains by AFM. *Science* 276:1109–1112.
39. Bustamante C, Marko JF, Siggia ED, Smith S (1994) Entropic elasticity of lambda-phage DNA. *Science* 265:1599–1600.
40. Levine ZA, Larini L, LaPointe NE, Feinstein SC, Shea J-E (2015) Regulation and aggregation of intrinsically disordered peptides. *Proc Natl Acad Sci USA* 112:2758–2763.
41. Möglich A, Joder K, Kiefhaber T (2006) End-to-end distance distributions and intrachain diffusion constants in unfolded polypeptide chains indicate intramolecular hydrogen bond formation. *Proc Natl Acad Sci USA* 103:12394–12399.
42. Rawat N, Biswas P (2014) Hydrogen bond dynamics in intrinsically disordered proteins. *J Phys Chem B* 118:3018–3025.
43. Fleming PJ, Rose GD (2005) Do all backbone polar groups in proteins form hydrogen bonds? *Protein Sc* 14:1911–1917.
44. Sheu S-Y, Yang D-Y, Selzle HL, Schlag EW (2003) Energetics of hydrogen bonds in peptides. *Proc Natl Acad Sci USA* 100:12683–12687.
45. Fersht AR, et al. (1985) Hydrogen bonding and biological specificity analysed by protein engineering. *Nature* 314:235–238.
46. Ragone R (2001) Hydrogen-bonding classes in proteins and their contribution to the unfolding reaction. *Protein Sci* 10:2075–2082.
47. Bolen DW, Rose GD (2008) Structure and energetics of the hydrogen-bonded backbone in protein folding. *Annu Rev Biochem* 77:339–362.
48. Knowles TPJ, et al. (2007) Kinetics and thermodynamics of amyloid formation from direct measurements of fluctuations in fibril mass. *Proc Natl Acad Sci USA* 104: 10016–10021.
49. Tsemekhman K, Goldschmidt L, Eisenberg D, Baker D (2007) Cooperative hydrogen bonding in amyloid formation. *Protein Sci* 16:761–764.
50. Knowles TP, et al. (2007) Role of intermolecular forces in defining material properties of protein nanofibrils. *Science* 318:1900–1903.
51. Zaccone A, et al. (2016) Kinetics of fragmentation and dissociation of two-strand protein filaments: Coarse-grained simulations and experiments. *J Chem Phys* 145: 105101.
52. Mannini B, et al. (2014) Toxicity of protein oligomers is rationalized by a function combining size and surface hydrophobicity. *ACS Chem Biol* 9:2309–2317.
53. Campioni S, et al. (2010) A causative link between the structure of aberrant protein oligomers and their toxicity. *Nat Chem Biol* 6:140–147.
54. Fauvet B, et al. (2012) a-Synuclein in central nervous system and from erythrocytes, mammalian cells, and Escherichia coli exists predominantly as disordered monomer. *J Biol Chem* 287:15345–15364.